Aligning Basilar Membrane Spirals to Two-Dimensional Images of Point-Stiffness Experiments

Graham E. Voysey,[1] Aleks Zosuls,[1] and Darlene R. Ketten[1, 2, 3]

[1]*Boston University Hearing Research Center and Department of Biomedical Engineering,*
44 Cummington Mall, Boston, MA 02215, USA
E-mail: gvoysey@bu.edu
[2]*Woods Hole Oceanographic Institution, Biology Department, Woods Hole, MA 02543, USA*
[3]*Department of Otology and Laryngology, Harvard Medical School, Boston, MA 02114, USA*

Abstract

Estimation of audiograms for marine mammals, particularly cetaceans, is a challenging task due to regulatory restrictions, sample availability, and the general paucity of data regarding the anatomical and physiological characteristics of the auditory system in these species. At present, we are characterizing point stiffness of the basilar membrane (BM), the principal resonating structure in the cochlea that supports hair cells of the organ of Corti. The ultimate goal of this project is to correlate point-stiffness measurements with accurate position-based estimates of the frequency response distribution along the BM in multiple cetacean species. Herein, we present the preliminary step of a method for estimating the length along the BM at which point-stiffness measurements were taken to determine frequency-stiffness correlates in one species, the harbor porpoise (*Phocoena phocoena*), which is also a "control" species for which there are live animal audiograms. A species-specific model of cochlear geometries and BM spirals were aligned and fitted to the individual curvature of each specimen on high-resolution photographs of the experimental point-stiffness measurement sites. This method produces reliable estimates of the location along the BM at which point stiffnesses were recorded, with precisions of approximately 0.33%, providing a reliable means of localizing point-stiffness responses for improving audiogram estimation.

Key Words: cetacean, hearing, modeling, basilar membrane, frequency-place map, cochlear length

Introduction

Conservation of marine mammal populations requires an understanding of the potential effects of anthropogenic sound on noise-exposed marine mammals. Critical to the prediction of such effects are reliable audiograms for marine mammal species, but directly obtaining audiograms from many species of key regulatory interest is often neither feasible nor practical. Our ultimate goal is to produce models of hearing that provide reliable estimates of audiograms for multiple marine species that cannot be tested by conventional audiometric means.

The basilar membrane (BM) is a tonotopically tuned system that vibrates with varying magnitudes along its length to incoming sounds (Yost, 1994). The fundamental action of the BM response is to transduce acoustic input pressures from the middle ear into action potentials. It determines a species' hearing range and sensitivities based on the BM tuning. The variations in motion of the membrane throughout the cochlea result in different degrees of flexion of cilia on hair cells atop the BM that, in turn, produce neural signals that are sent to the auditory centers in the brain. Thus, the BM separates complex sounds into their component frequencies, and the position and degree of flexion result in the ability to detect frequencies and relative intensities of the incoming sounds. Having knowledge of the mapping of frequency response to location along the length of the BM is a key element for modeling hearing frequency range, sensitivity, and frequency discrimination of the inner ear. These parameters are fundamental to estimating how noise affects the ear of any given species. Frequency mapping has a long history, beginning with the work of Stacey R. Guild (1927) as well as others (Greenwood, 1961; West, 1985; Ketten et al., 1998; Mountain et al., 2003). Each of these provide a number of cochlear measures that correlate with the hearing ranges and frequency distributions for a variety of species.

We developed models from a combination of experimental, physiological, and anatomical measures. We used a functional, biophysical system approach in which the hearing apparatus is divided into external-, middle-, and inner-ear components.

Stiffness and mass of middle- and inner-ear components are critical features that determine the breadth and sensitivity of hearing in any species and, indeed, in each individual. The work discussed herein focuses on estimating the locations of direct mechanical stiffness measurements taken along the length of the BM in the inner ear.

Methods

Point-Stiffness Experimental Data

Point-stiffness experimental data employed in this project were obtained by nano-indentation force probe measures in cochleae extracted *postmortem* as reported previously (Tubelli et al., 2012, 2018). The point-stiffness measurements, in combination with BM dimensions, are inputs to a model to predict the frequency-place map of the cochlea (Zosuls et al., 2012). The frequency-place map indicates where along the BM resolvable frequencies (i.e., those within the tuning of that membrane in each species) will produce a maximal response. It is the site of the first point of tonotopic mapping in the auditory system, which is also a characteristic of higher auditory centers such as those in the brainstem and the auditory cortex (Kollmeier, 2008). Establishing the frequency-place map is, therefore, fundamental for the estimation of audiograms.

Our database of point-stiffness measurements, to date, were obtained from experiments on 90 specimens from nine mammalian species (22 marine mammal, 59 rodent, and nine human ears). Experimental data for each specimen included point-stiffness measurements taken with a custom probe across the entire width of the BM at multiple longitudinal locations along the cochlear spiral, as well as photographs taken during the experiment. Also included were metadata about the animal, its condition, tissue preservation, and other life history information. The transaxial stiffness profile at each site on the BM may also be used to estimate the width of the BM at each longitudinal location.

We developed a data alignment tool and methodology to calculate where along the BM point-stiffness measurement sites were located. This tool allows an initial approximation of the spiral path for the BM to be overlain and aligned with two-dimensional (2D) planar photos taken during each point-stiffness experiment of the temporal bone with openings into the cochlea. The spiral configuration employed for each specimen was based on anatomical measures described in the following section. The data alignment tool estimates the location along the BM in millimeters from the oval window for each opening site along the cochlea where the force probe was placed for point-stiffness measurements. This provides a method by which an individualized BM spiral is generated as an overlay of cochlear point-stiffness measurement sites taken *in situ* during experiments.

Species-Specific Spirals Are Obtained from Anatomical Data

Anatomical measurements of the ears of harbor porpoise (*Phocoena phocoena*) specimens were extracted from computerized tomography scans and spiral morphometric analyses published in prior studies (Ketten & Wartzok, 1990; Ketten, 1994) as well as from recent specimen examinations. In this article, we focus on examples of the analyses for the harbor porpoise. It is a key control animal for the model in that it has been studied well both anatomically and audiometrically, with multiple high-quality tissue datasets available. Additionally, the relatively planar nature of the Type I cochlear spiral (Ketten, 1992) in *P. phocoena* is well suited to 2D reconstruction with minimal loss of fidelity from angular distortions.

We digitized the cochlear spiral plots for previously published 2D and three-dimensional (3D) cochlear images using a graphic reconstruction tool (Rohatgi, 2019) to generate discrete data points that described the spatial geometry of the BM of each cochlea. We selected this digitization tool because it takes into account planar distortions and skew of plot visualizations with minimal error (average of 0.25%) during reconstruction (Burda et al., 2017).

Characteristic continuous equations describing spirals as they were described in Ketten & Wartzok (1990) were generated from the reconstructed x and y coordinates of the anatomical data. Data points were fit to the spiral equations corresponding to cochlear spiral types for each species with the *MATLAB* 'fminsearch' tool (Mathworks, 2018), an implementation of the nonlinear Neadler-Mead simplex routine (Lagarias et al., 1998). This approach provides a robust fitting approach—that is, at most, only small variations in starting conditions that do not alter final states and which, therefore, do not result in any evident dependence on initial conditions. For *P. phocoena*, the root-mean-squared (rms) error between the original data and the spiral equation was 0.187.

Spirals Are Aligned to Images with a State-Space Search

To optimize the alignment of the estimated spiral, we employed a state-space search, which is a procedure commonly applied in artificial intelligence and machine learning. The essence of this approach is to consider and iteratively compare successive potential configurations (states) of possible values to determine what combination of

values (search) for a regular spiral path provides the least composite error over all data points subject to the constraints of an optimization function, which defines which error metric to use. This provides a best fit and alignment of the output spiral to the experimental image.

Figure 1 shows the progressive alignment of the spiral from a constrained state-space search in the immediate neighborhood of a user-selected initial spiral position. Candidate alignments are constrained by default to those within ±10° of rotation and a circle with a 50-pixel radius in which the spiral center point is free to move. To facilitate fitting spirals to images of many resolutions, the constraints for the state-space search are user-configurable. Beginning from a user-selected initial spiral placement, this process simplified our approach by eliminating spurious spiral alignments that could arise with a naive fitting algorithm. This approach can potentially converge on local minima; however, we address this by providing user interface controls so that the initial spiral location that the user selects is in a location in the state space where any local minimum is also the desired alignment. In the case of *P. phocoena*, 2D fits are an acceptable approximation of the actual shape because of the nearly planar, low axial height of the porpoise cochlea.

We defined our objective function to be the summed Euclidean distance between the labelled point-stiffness measurement sites and the nearest point on the spiral. The spiral was rotated, translated, and linearly scaled across the underlying image such that this objective function is minimized. With the spiral scaling and chirality pre-established by the user, we successively selected potential rotation and center positions and searched the state space. Final alignment was obtained by selecting the combination of rotation angle and spiral center-point parameters that minimized the summed Euclidian distance of the nearest point on the spiral to each of the user-selected points that correspond to a point-stiffness measurement location on the image.

Aligned Spirals Are Used to Estimate the Location of Measurement Sites
With the spiral alignment complete, the location, both in absolute terms and as a percentage along the basal-apical length, was computed by measuring the arc length of the spiral for the entire length, as well as the incremental length to each of the selected point-stiffness measurement sites. We used *MATLAB*'s piecewise cubic hermite interpolating polynomial (pchip) method to approximate arc length as it preserves data shape and monotonicity.
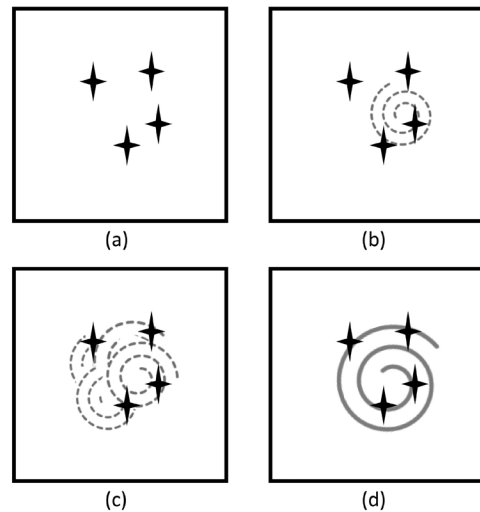

Figure 1. Guided state-space search fitting algorithm for spiral alignment: (a) Ground-truth markers (black stars) of the alignment sites were specified by the user on the plane and corresponded to locations on an image of tissue (not pictured) where point-stiffness measurements were taken; (b) an initial reasonable-guess placement of a spiral was then made; (c) a rapid search for a best fit was made by varying the spiral rotation and center location—for each iteration, the summed Euclidean distance between the marker points was computed; and (d) the spiral with center location and rotation that best minimized the Euclidean distance was preserved as the best alignment.

Results

We tested that our spiral fitting approach was resilient to small perturbations in the selection of measurement sites on the image with a sensitivity analysis (Figure 2). First, the user-selected point-stiffness measurement sites were randomly reassigned to new locations within a circle of ~0.6 mm radius from their initial locations, and the fitting procedure was re-run. For $n = 50$ runs in which four marker points were thus dithered, the mean summed distance between the spiral and points was 0.41 mm with a standard deviation (SD) of 0.06 mm. The low variation in mean summed distance indicates that our approach is stable and does not produce spurious results given small changes in initial conditions that are user-driven. Second, the percentage length assigned to each point-stiffness measurement site varied little. For four point-stiffness measurement sites, the SDs across 50 perturbations had a mean value of 0.33% (SD = 0.13). This indicates that not only does the method align spirals to points with high affinity—that is, the mean distance is small—it
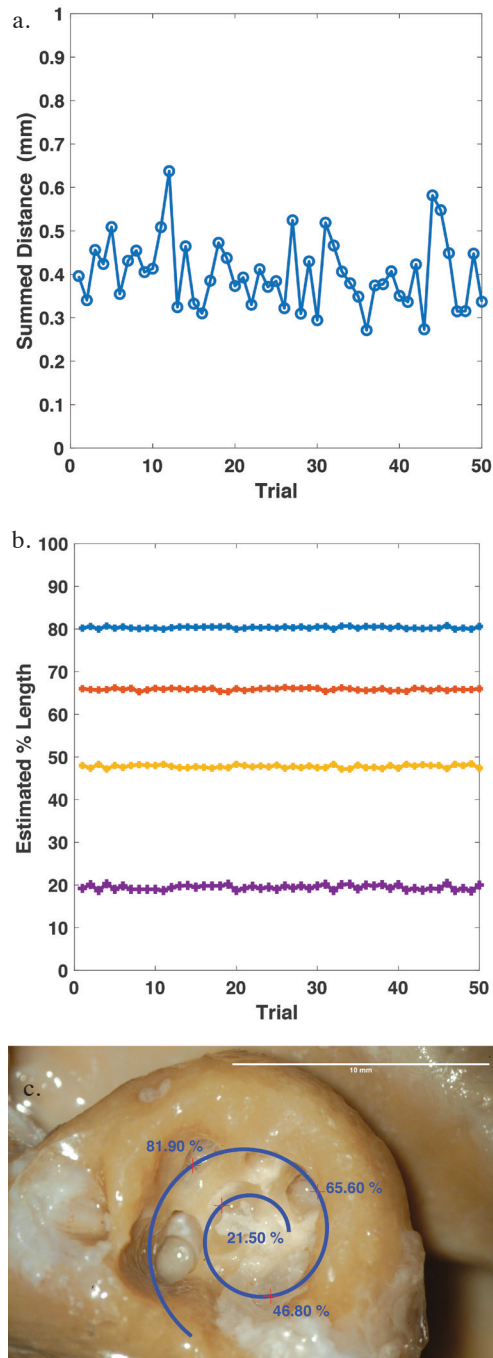
Figure 2. (a) Spiral alignment is not sensitive to small perturbations in initial anchor point locations; (b) over 50 random perturbations, the best fit remains stable and tightly localized; and (c) the final estimated percentage of length. The estimated percentage of each basilar membrane (BM) length for four anchor point locations remains consistent (mean SD = 0.336%).

also robustly preserves the estimated length assignment for each point. This is especially important due to the nonlinear frequency-place mapping along the BM, where small changes in location result in large changes in estimated best frequency (Oghalai, 2004). In this work, we are characterizing the stiffness—a passive material property of the BM. While the BM has sharply tuned responses about the characteristic frequency at a particular location, this may be the effects of the cochlear amplifier (Oghalai, 2004), an active process that augments the more slowly varying material properties of the BM itself. With total BM length on the order of 20 to 25 mm in this species, a variation in estimated percentage length on the order of 60 microns is small.

Discussion

The method of spiral alignment and fitting detailed herein prepares us for the future work of synthesizing multiple independent methods to predict audiograms for each challenging marine mammal species. In the current work, we focused on estimation of best frequency from point-stiffness measurements taken across cross-sectional widths of the BM at many different basal-apical locations along the spiral. The locations where these point-stiffness measurements are taken need to be considered in their anatomical context. Not only are the stiffness of the tissues important for prediction of best frequencies, but also the locations of where measured tissues lie along the BM must be determined with high fidelity for an accurate frequency-place map to be obtained.

Precisely identifying the exact pixel site at which an experimental measurement was taken is not feasible for a number of reasons: pixel densities in computer monitors are non-uniform across displays; users may use more or less care in labeling sites; and any given site selection may cover a broad, multi-pixel image area. In addition, the point-stiffness probe has physical dimensions that occupy an area of the image that covers more than a single pixel, so selecting a single pixel is not representative of the realities of the experiment. The stability and precision of our estimates of location are such that it is appropriate to use this tool across a wide range of computers, displays, and photograph resolutions. At least three sites should be identified on the image as anchor points to obtain reliable results; these must be separated enough along the spiral so that spurious fits are not generated.

A further goal is to compare the stiffness-derived best frequency estimates to previously established methods such as membrane place-mapping approaches (Guild, 1927; West, 1985; Ketten, 1994; Ketten et al., 1998) noted above.

This method will help address issues of data and tissue quality for species of critical regulatory interest such as mysticetes. Combining multiple independent modalities of frequency-place mapping with reliably localized experimental sites lets us address samples with variable tissue quality or other common sample imperfections.

Our long-term goal is to obtain multiple independent and reliable anatomical and modeling measures and combine them into estimates of the audiogram across multiple species. We are focused currently on critically undocumented species that present unique challenges for direct audiometric study, such as the largest baleen whales, but this method is suitable for use with any mammalian species, particularly those for which there are control audiograms to test the validity of this approach. In the case of cetaceans, *P. phocoena* is one such control species as well as bottlenose dolphins (*Tursiops truncatus*). Some challenges include the difficulties of obtaining specimens of adequate quality for nano-indentation experiments as well as the technical difficulties of high-resolution imaging on very large specimens. A reliable means of assigning a cochlear length for a given point-stiffness experimental measurement dataset opens a new avenue of investigation and provides an opportunity to synthesize multiple independent measurements of cochlear responses into a more accurate framework for this goal.

Acknowledgments

Literature Cited

Burda, B. U., O'Connor, E. A., Webber, E. M., Redmond, N., & Perdue, L. A. (2017). Estimating data from figures with a Web-based program: Considerations for a systematic review. *Research Synthesis Methods*, 8(3), 258-262. https://doi.org/10.1002/jrsm.1232

Greenwood, D. D. (1961). Auditory masking and the critical band. *The Journal of the Acoustical Society of America*, 33(4), 484-502. https://doi.org/10.1121/1.1908699

Guild, S. R. (1927). The width of the basilar membrane. *Science*, 65(1673), 67-69. https://doi.org/10.1126/science.65.1673.67

Ketten, D. R. (1992). The marine mammal ear: Specializations for aquatic audition and echolocation. In D. B. Webster, A. N. Popper, & R. R. Fay (Eds.), *The evolutionary biology of hearing* (pp. 717-750). New York: Springer. https://doi.org/10.1007/978-1-4612-2784-7_44

Ketten, D. R. (1994). Functional analyses of whale ears: Adaptations for underwater hearing. *Proceedings of OCEANS'94*, 1, I/264-I/270. https://doi.org/10.1109/OCEANS.1994.363871

Ketten, D. R., & Wartzok, D. (1990). Three-dimensional reconstructions of the dolphin ear. In J. A. Thomas & R. A. Kastelein (Eds.), *Sensory abilities of cetaceans: Laboratory and field evidence* (pp. 81-105). New York: Springer. https://doi.org/10.1007/978-1-4899-0858-2_6

Ketten, D. R., Skinner, M. W., Wang, G., Vannier, M. W., Gates, G. A., & Neely, J. G. (1998). *In vivo* measures of cochlear length and insertion depth of nucleus cochlear implant electrode arrays. *The Annals of Otology, Rhinology & Laryngology (Supplement)*, 175, 1-16. Retrieved from www.ncbi.nlm.nih.gov/pubmed/9826942

Kollmeier, B. (2008). Anatomy, physiology and function of the auditory system. In D. Havelock, S. Kuwano, & M. Vorländer (Eds.), *Handbook of signal processing in acoustics* (pp. 147-158). New York: Springer. https://doi.org/10.1007/978-0-387-30441-0_10

Lagarias, J. C., Reeds, J. A., Wright, M. H., & Wright, P. E. (1998). Convergence properties of the Nelder-Mead Simplex Method in low dimensions. *SIAM Journal on Optimization*, 9(1), 112-147. https://doi.org/10.1137/S1052623496303470

Mathworks. (2018). *MATLAB release 2018a*. Natick, MA: The Mathworks Inc.

Mountain, D. C., Hubbard, A. E., Ketten, D. R., & O'Malley, J. T. (2003). The helicotrema: Measurements and models. *Biophysics of the Cochlea*, 393-399. https://doi.org/10.1142/9789812704931_0053

Oghalai, J. S. (2004). The cochlear amplifier: Augmentation of the traveling wave within the inner ear. *Current Opinion in Otolaryngology & Head and Neck Surgery*, 12(5), 431-438. Retrieved from www.ncbi.nlm.nih.gov/pubmed/15377957

Rohatgi, A. (2019). *WebPlotDigitizer*. Retrieved from https://automeris.io/WebPlotDigitizer

Tubelli, A. A., Zosuls, A., Ketten, D. R., & Mountain, D. C. (2018). A model and experimental approach to

the middle ear transfer function related to hearing in the humpback whale (*Megaptera novaeangliae*). *The Journal of the Acoustical Society of America*, *144*(2), 525-535. https://doi.org/10.1121/1.5048421

Tubelli, A. A., Zosuls, A., Ketten, D. R., Yamato, M., & Mountain, D. C. (2012). A prediction of the minke whale (*Balaenoptera acutorostrata*) middle-ear transfer function. *The Journal of the Acoustical Society of America*, *132*(5), 3263-3272. https://doi.org/10.1121/1.4756950

West, C. D. (1985). The relationship of the spiral turns of the cochlea and the length of the basilar membrane to the range of audible frequencies in ground dwelling mammals. *The Journal of the Acoustical Society of America*, *77*(3), 1091-1101. https://doi.org/10.1121/1.392227

Yost, W. A. (1994). *Fundamentals of hearing* (3rd ed.). San Francisco, CA: Academic Press.

Zosuls, A., Newburg, S. O., Ketten, D. R., & Mountain, D. C. (2012). Reverse engineering the cetacean ear to extract audiograms. In A. N. Popper & A. Hawkins (Eds.), *The effects of noise on aquatic life: Advances in experimental medicine and biology* (Vol. 730, pp. 61-63). New York: Springer. https://doi.org/10.1007/978-1-4419-7311-5_13